Liquid Crystals
Publication details, including instructions for authors and subscription information:
http://www.tandfonline.com/loi/tlct20

Analysis of the performance of the electric-field-driven liquid crystal lens (ELC Lens) for light of various incident angles

HyungKi Hong [a]

[a] Department of Optometry, Seoul National University of Science and Technology, Nowon-gu, Seoul, Republic of Korea

Version of record first published: 08 Jun 2012

To cite this article: HyungKi Hong (2012): Analysis of the performance of the electric-field-driven liquid crystal lens (ELC Lens) for light of various incident angles, Liquid Crystals, 39:9, 1055-1061

To link to this article: http://dx.doi.org/10.1080/02678292.2012.696732

Liquid Crystals,
Vol. 39, No. 9, September 2012, 1055–1061

Taylor & Francis
Taylor & Francis Group

Analysis of the performance of the electric-field-driven liquid crystal lens (ELC Lens) for light of various incident angles

HyungKi Hong*

Department of Optometry, Seoul National University of Science and Technology, Nowon-gu, Seoul, Republic of Korea

(*Received 4 May 2012; final version received 21 May 2012*)

The electric-field-driven liquid crystal lens (ELC) induces the lens effect by the spatially non-uniform distribution of the refractive index. A scheme to analyse the performance of the ELC lens for the lights of various incident angles is devised by the calculation of the phase through the ELC lens and the determination of light ray directions from these phases. The calculated results show that the ELC lens changes the incident light of the plane wave into a focused wave and the focal distance becomes shorter for larger incident angles.

Keywords: controllable lens; liquid crystal lens; light ray; wave front; autostereoscopic 3D; GRIN lens

1. Introduction

Nowadays, 3D technologies are often used in 3D theatre and some 3D TV [1, 2]. However, most of the current commercialised 3D technologies require the user to wear special eyeglasses to perceive the depth. Autostereoscopic 3D is one category of 3D technologies where no special eyeglass is necessary to perceive the depth. Autostereoscopic 3D typically uses the configuration where the optical elements such as the parallax barrier or the cylindrical lens are placed in front of the imaging displays [1]. To realise the 2D/3D switching, various technologies have been reported such as the change of the refractive index of a liquid crystal (LC) at the lens-shaped boundary or the change of the incident polarisation direction passing through an anisotropic lens [3–5].

One of these reported technologies is the electric-field-driven LC lens (ELC lens), based on the principle of the gradient index (GRIN) lens [6, 7]. The principle of the ELC lens is illustrated in Figure 1. In an ELC lens, the non-uniform electric field distributions induce the non-uniform alignment of LC directors and the non-uniform distribution of the effective refractive index n_{eff} of the LC. The spatial non-uniformity of n_{eff} determines the shape of the wave front and the light ray direction, similar to the principle of a GRIN lens.

The performance of the lens for obliquely incident light is important, especially for display applications where the viewer's position is not strictly restricted to one position. Moreover, it is already well known that the n_{eff} value of a LC is dependent on the direction. Hence it is expected that the characteristics of an ELC lens may be affected by the direction of the incident light. The analysis of the angular dependence of the GRIN lens by the Hamiltonian method was recently reported [8]; however, more research is needed to fully understand the performance of the lens and the path of the light rays, especially for the light incident on the edge of lens.

How the lights of different incident angles are affected by an ELC lens is investigated in this paper. Firstly, the distribution condition of the alignments of the LC directors is adjusted to match the shape of the intended phase for the case of the incident angle of 0°. For this condition, the phase of the propagating light throughout the ELC lens is calculated for the various incident angles using the Jones matrix method. Then, from these calculated data of the spatial phase distribution, light ray directions are derived and, finally, how the lights focus is investigated.

2. Theory

The usefulness of a switchable cylindrical lens is especially important for 2D/3D display and research into a switchable cylindrical lens has been reported [9, 10]. In this paper, an ELC lens that induces the effect of the cylindrical lens is considered. The coordinate system is selected such that the direction of the infinite radius of lens is along the y-direction as illustrated in Figure 2(a). It is assumed that the thickness of the LC cell of the ELC lens is much smaller than the focal length of the lens and hence the propagating direction of light does not change inside the LC cell. As ELC lenses use the spatial distribution of the refractive index to induce the lens effect, the lens effect is affected by the light path inside the ELC lens. Figure 2(a) illustrates the light path for the normally and the obliquely incident light. It is assumed that the incident light of

*Email: hyungki.hong@snut.ac.kr

ISSN 0267-8292 print/ISSN 1366-5855 online

http://dx.doi.org/10.1080/02678292.2012.696732
http://www.tandfonline.com

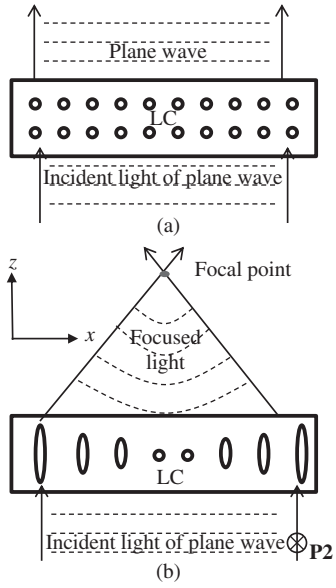

Figure 1. The principle of the ELC lens using the spatial distribution of the refractive indices which are caused by the spatially non-uniform LC alignments. (a) Lens-OFF state and (b) Lens-ON state. **P2** represents the polarisation state along the *y*-axis.

linear polarisation of the *y*-direction is on the *xz*-plane, the direction of normal incidence is parallel to the *z*-axis and LC directors are aligned homogeneously along the *y*-axis. In the case of normal incidence, the *x*-coordinate of the light path does not change inside the ELC lens and the wave front of the same phase, irrespective of the *x*-coordinate, is incident on the lower side of the substrate if the incident light is a plane wave. However, in the case of the non-zero incident angle θ_{in}, the *x*-coordinate of the light path changes as $x_{\text{i}} + z\ \sin(\theta_{\text{r}})$ inside the ELC lens, where θ_{r} is the refractive angle. Also, when the plane wave is incident on the lower side of the substrate, the phase difference of $k(x_2 - x_1)\sin(\theta_{\text{in}})$ exists between x_1 and x_2. These two factors should be considered in calculating the phase profile of the ELC lens for oblique incidence.

The LC distribution of ELC lens can be treated as *M* by *N* meshes of a finite size where each mesh is a uniform uniaxial medium as illustrated in Figure 2(b). When the thickness of the LC cell gap is z_N, the LC cell can be treated as the combination of *N* layers with thickness $(z_N)/N = \Delta z$. When the light is incident at the position of $(x_1, 0)$ on the side of the lower substrate, coordinate (x_p, z_p) of the light path at the *p*-th layer along the *z*-direction is determined as follows.

$$x_p = x_1 + Z_p\ \sin(\theta_{\text{r}}) = x_1 + p\Delta z \sin(\theta_r) \qquad (1)$$

If the distribution of the LC directors of the ELC lens is known, the effective refractive index n_{eff} for each

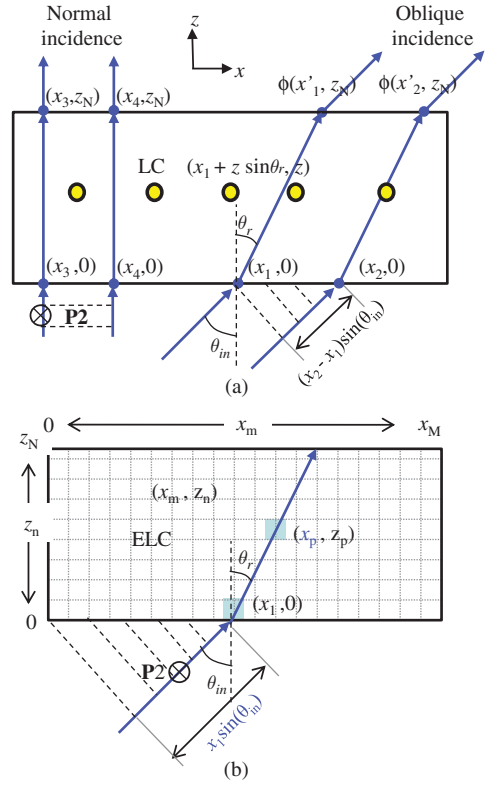

Figure 2. (a) Comparison of the light path between the normal and the oblique incidence. When the positions from which light enters the LC layer are different, these cause the addition phase change $k(x_2 - x_1)\sin(\theta_{\text{in}})$ for the plane wave of oblique incidence. (b) Propagation of the light with the incident angle θ_{in} through an ELC layer which is treated as an *M* by *N* matrix. (x_p, z_p) of light path can be determined from the incident angle θ_{in} and the position x_1.

condition of the different incident angle can be determined at (x_p, z_p) of the light path. The phase change at the position (x_p, z_p) by each mesh of the uniaxial medium can be written in Jones matrix representation as follows [11]:

$$\boldsymbol{M}(x_1, x_p, z_p) = \boldsymbol{R}(-\phi_2(x_p, z_p))\,\boldsymbol{P}(x_p, z_p)\,\boldsymbol{R}(\phi_2(x_p, z_p)). \qquad (2)$$

The rotation matrix $\boldsymbol{R}$ and propagation matrix $\boldsymbol{P}$ are

$$\boldsymbol{R}(\phi_2) = \begin{pmatrix} \cos\phi_2 & \sin\phi_2 \\ -\sin\phi_2 & \cos\phi_2 \end{pmatrix}$$

$$\boldsymbol{P}(x_p, z_p) = \begin{pmatrix} \exp\left(-i\frac{2\pi\,\Delta z n_o}{\lambda}\right) & 0 \\ 0 & \exp\left(-i\frac{2\pi\,\Delta z n_{\text{eff}}(x_1, x_p, z_p)}{\lambda}\right) \end{pmatrix} \qquad (3)$$

Here, λ represents the wavelength. Then, the overall phase change that occurs as the light passes through z_N layers can be derived from the successive multiplication of these matrices.

$$\boldsymbol{M}(x_1) = \sum_{z_p=0}^{z_N} M(x_1, x_p, z_p) \tag{4}$$

From equation (4) of the matrix multiplication, the phase induced by the ELC lens can be calculated for each position where x_1 is the x-coordinate of the position from which light enters the LC cell.

As for the second factor, that the phase difference exists on the side of the lower substrate, the phase difference is calculated with respect to the left boundary of the ELC lens. Therefore the phase difference between the light at positions (x_1, 0) and (0, 0) can be written as $kx_1\sin(\theta_{\text{in}})$.

3. Simulation

Commercial software (Techwiz 2D) is used to calculate the M by N matrix of LC director distributions under the electric field to induce the cylindrical lens effect by an ELC lens [12]. The ELC structure used for the simulation is illustrated in Figure 3. Infinite length is assumed along the y-direction, so electrodes of infinite length along the y-direction are assumed and LC distribution along the y-direction is not considered. In addition, the periodic boundary condition is used along the x-direction. The pitch of each cylindrical lens is selected as $x_M = 0.2$ mm in consideration of an autostereoscopic 2-view display where each pixel consists of RGB subpixels of the vertical stripe type and the subpixel pitch of the imaging display is 0.1 mm. The focal length of the cylindrical lens is selected as $f = 1.7$ mm to make the designed viewing distance 1100 cm. The phase change caused by a lens of focal length f and lens pitch x_M can be written as follows [7]:

$$\Delta\phi = kx_{\text{L}}^2/2f, 0 < x_{\text{L}} < x_M/2. \tag{5}$$

Here, x_L is the distance from the center of the lenticular lens along the x-direction. From this equation, the maximum phase change is $\Delta\phi = 34$ radians at $x_L = 0.1$ mm. The refractive indices of the LC used for the simulation are refractive index of extraordinary wave $n_{\text{e}} = 1.5977$ and refractive index of ordinary wave $n_{\text{o}} = 1.4828$. The thickness of the LC cell is selected as 50 μm to induce a phase change similar to the maximum phase change of equation (5). As the maximum phase change is determined by the birefringence and the cell gap, a LC of higher birefringence will result in a thinner cell gap and maybe a faster response [13]. As the focal length of the lens $f = 1.7$mm is much larger than the thickness of the LC cell of ELC lens, it is assumed that the propagating direction of light does not change inside the LC cell. LC directors are selected to be homogeneously aligned along the y-direction. Other material parameters of LC used for the simulation are the dielectric constant for extraordinary wave $\varepsilon(\text{e}) = 8.3$ and the dielectric constant for ordinary wave $\varepsilon(\text{o}) = 3$, and elastic constants $K_{11} = 13$ pN, $K_{22} = 5.8$ pN, $K_{33} = 12.7$ pN. On the side of the upper substrate, 20 electrodes of 5 μm width are placed at distances of 5 μm. These electrodes are connected to different voltage levels to induce a spatially non-uniform electric field. On the side of the lower substrate, a non-patterned electrode is placed and connected to the ground voltage. By the adjustment of the voltages connected to the patterned electrodes on the side of the upper substrate, the distribution of the LC directors is determined, which induces the phase profile of focal length $f = 1.7$mm for normally incident light [14]. The voltage levels applied to each patterned electrode on the side of the upper substrate are presented in Table 1.

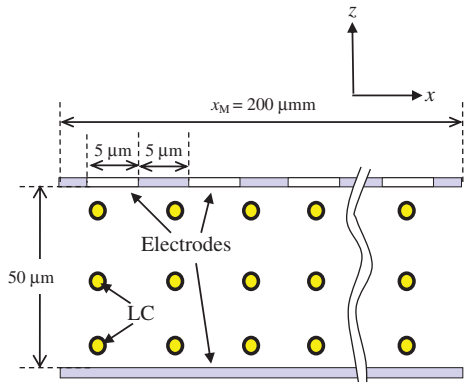

Figure 3. Configuration of the LC cell and the electrode structure of the ELC lens. Electrodes on the side of the upper substrate are patterned with an interval of 5 μm and a width of 5 μm. These electrodes are connected to different voltage levels to induce a non-uniform electric field. The electrode on the side of the lower substrate is connected to the ground voltage. LC directors of positive $\Delta\varepsilon$ are initially aligned homogeneously.

With respect to this distribution of LC directors, the dependence of the ELC lens is analysed as the incident angle θ_{in} is changed from 0° to 60°. The phase changes at position x_p along the light path are calculated using equations (1) and (4). In the ELC configuration, $n_{\text{e}} = 1.5977$, $n_{\text{o}} = 1.4828$, the thickness of the LC cell is 50μm and the LCs are initially homogeneously aligned. In this configuration, the x-coordinates of the e-wave and the o-wave that

Table 1. Voltage levels applied to the electrodes on the side of the upper substrate. The positions of electrodes 11 and 1 correspond to the centre and the boundary of the lens respectively [14].

Electrode	1	2	3	4	5	6	7	8	9	10	11	12	13	14	15	16	17	18	19	20
Voltage	3.3	2.7	2.5	2.3	2.2	2.1	2.0	1.8	1.6	1.3	1.0	1.3	1.6	1.8	2.0	2.1	2.2	2.3	2.5	2.7

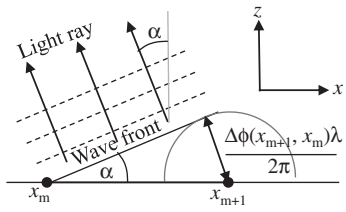

Figure 4. Scheme to determine the light ray direction from the phase difference between two positions x_m and x_{m+1}.

exit the LC cell are different by 13.6 μm and 14.6 μm from the entry position of $(x_1, 0)$ for the incident angle of 60°. It means that the difference in the light path between the e-wave and the o-wave is less than 1 μm when the incident angle is smaller than 60°. Therefore, the light paths of the e-wave and the o-wave are assumed to be equal inside the LC cell. As the incident polarisation of the y-direction is parallel to the optic axis of the LC, the refractive index is assumed to be n_e of the LC for Snell's Law of $\sin(\theta_{in}) = n_e \sin(\theta_r)$ and this refractive angle is used for equation (1). Once the phases inside the LC cell are calculated, the phase of $kx_1\sin(\theta_{in})$ is added as well in order to estimate the direction of the light ray.

Figure 4 illustrates the scheme to determine the wave front and the light ray direction from the phases of two positions x_m and x_{m+1}. When the phase difference between two positions x_m and x_{m+1} is $\Delta\phi(x_m, x_{m+1})$, the position that is distant from x_{m+1} by $\Delta\phi(x_m, x_{m+1})/k = \Delta\phi(x_m, x_{m+1})\lambda/2\pi$, will have the same phase as position x_m. From this, the wave front of the equal phase can be determined. Then the angle α that represents the propagating direction of the wave front in Figure 4 can be determined. As the propagating direction of the wave front is equal to the direction of the light ray at each position, the directions of light rays from the spatially non-uniform phase profile can be determined.

4. Results and Analysis

Figure 5 illustrates the calculated phase caused by the LC layer of the ELC lens for the different incident angles. The phase at the lower boundary of the LC layer is selected as zero. In Figure 5, the symmetric axes of the phase profiles are shifted for larger incident angles. These shift can be attributed to the fact that the x-coordinate of the light path changes from

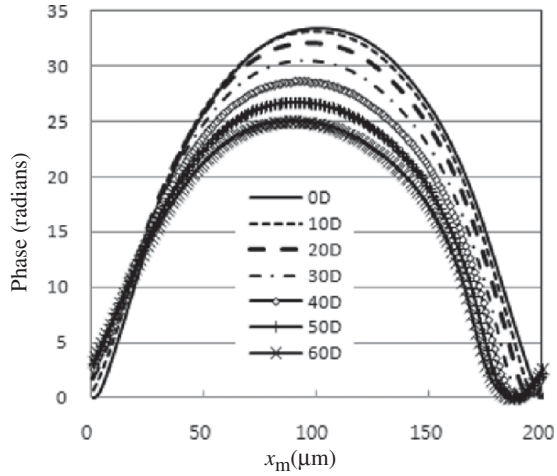

Figure 5. Spatial phase distribution caused by the LC layer of the ELC lens for various incident angles. Numbers in the lower centre of the figure represent the incident angles. The horizontal and vertical axes represent the x-position and the phase, respectively.

x_1 to $x_p = x_1 + z_p \sin(\theta_r)$. Figure 5 also shows that the maxima of the phases are observed to decrease for larger incident angles. However, the wave fronts are determined not by the maximum value of the phase, but the shape of the phase curve. So each phase curve of Figure 5 is modified such that the horizontal positions of the maximum phases of each curve are shifted to be the same position and the maxima of each curve are matched. The results are illustrated in Figure 6. Figure 6 shows that the phase profile of the larger incident angle becomes less steep farther from the maximum position. This can be attributed to the fact that the obliquely propagating light passes horizontally through the region of the different refractive indices.

From the result of the calculated phase curve, light ray directions are determined by the scheme illustrated in Figure 4. Figure 7 illustrates the calculated result of the light ray direction and the light ray's focusing characteristics on the zx-plane for an incident angle of 0°. From the data on the phase at each horizontal position, the angle of the light ray direction is determined at the horizontal interval of 1 μm as illustrated in Figure 7(a). Then the path of light ray coming from position x_m is drawn on the zx-plane for the horizontal interval of 5 μm as illustrated in Figure 7(b). The phases are calculated to be symmetric with respect to $x_m = 100$ μm and the light ray at $x_m = 100$ μm

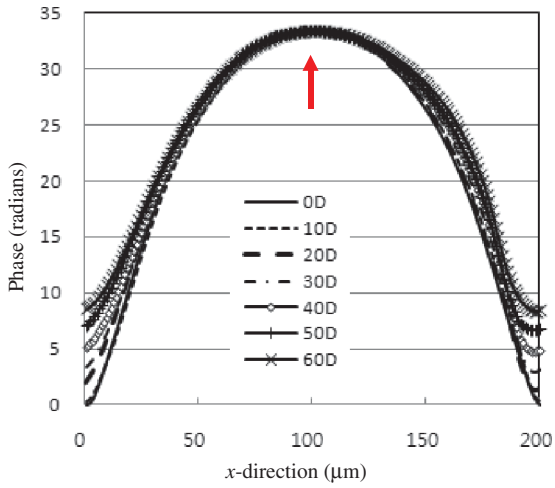

Figure 6. Spatial phase distribution where the curve of Figure 5 is modified such that the horizontal position and maximum phase are at the same point. Numbers in the lower centre of the figure represent the incident angles. The horizontal and vertical axes represent the x-position and the phase, respectively.

propagates along the z-axis. As the designed ELC lens structure is symmetric with respect to the position of $x_m = 100$ μm, the optic axis of the lens can be considered to pass through the position of $x_m = 100$ μm and to be parallel to the z-axis.

In Figure 7(b), the light rays show the trend of focusing around the z-coordinate of 1800 μm when the x-coordinate of the incident position is near the optic axis. However, the light rays coming from the x_m position smaller than 50 μm or larger than 150 μm tend to pass through the optic axis at the shorter distance. That the focal length becomes shorter for the light that is incident parallel to the optic axis and far from the optic axis of the lens is generally called spherical aberration [15]. The analysis of the light ray direction shows that the focusing characteristics of the lens becomes less uniform as the x_m position becomes farther from the optic axis of $x_m = 100$ μm. This can also provide the information about the horizontal range of ELC lens which can be utilised.

The position at which light rays intersect the optic axis can be derived from x_m and the angle of the light ray. If the light ray from any position x_m intersects the optic axis of the lens at the same position, this intersecting position is the focus of the lens. Then, the following relations will be held as illustrated in Figure 8(a).

$$f = \frac{(100 - x_a)}{\tan\beta(x_a)} = \frac{(100 - x_b)}{\tan\beta(x_b)} \tag{6}$$

Here β represents the angle of the light ray for the lens where the focal position is f irrespective of x_m. From equation (6), angle β is derived to be quite linear

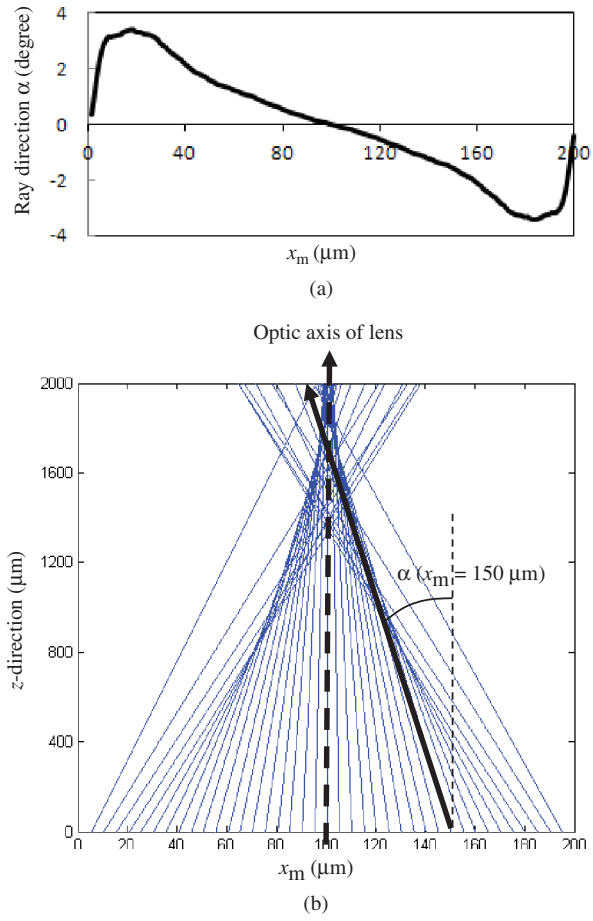

Figure 7. Calculation of the path of light rays from the spatial phase distribution of the incident angle of 0°. (a) Angle of the light rays after the light passes through the ELC lens. (b) Light rays after the light passes through the ELC lens on the zx-plane. The ELC lens is located at 0 mm in the z-direction and at x-coordinate ranges of 0–200 μm. The structure of the ELC lens is symmetric with respect to the x-coordinate of $x_m = 100$ μm.

as illustrated in Figure 8(b). Comparison of angle β with the angle α induced by the ELC lens shows that the difference between the two angles becomes noticeable as the x_m position becomes smaller than 50 μm or larger than 150 μm.

By the same procedure described above, the light ray paths are also determined for the oblique incidences where the incident angle θ_{in} is not zero. The results are illustrated in Figure 9. The angle of the light ray direction is determined from the sum of the phase of the ELC lens and $kx_1\sin(\theta_{in})$. The first part mostly determines the focusing characteristics; the second part plays the role of rotating the wave front at each position by an amount similar to the incident angle.

The angles of light rays from the ELC lens are illustrated in Figure 9(a). The curves of the angles are linear near the optic axis where x_m is 100 μm but as x_m becomes farther from 150 μm, the curves of the angles

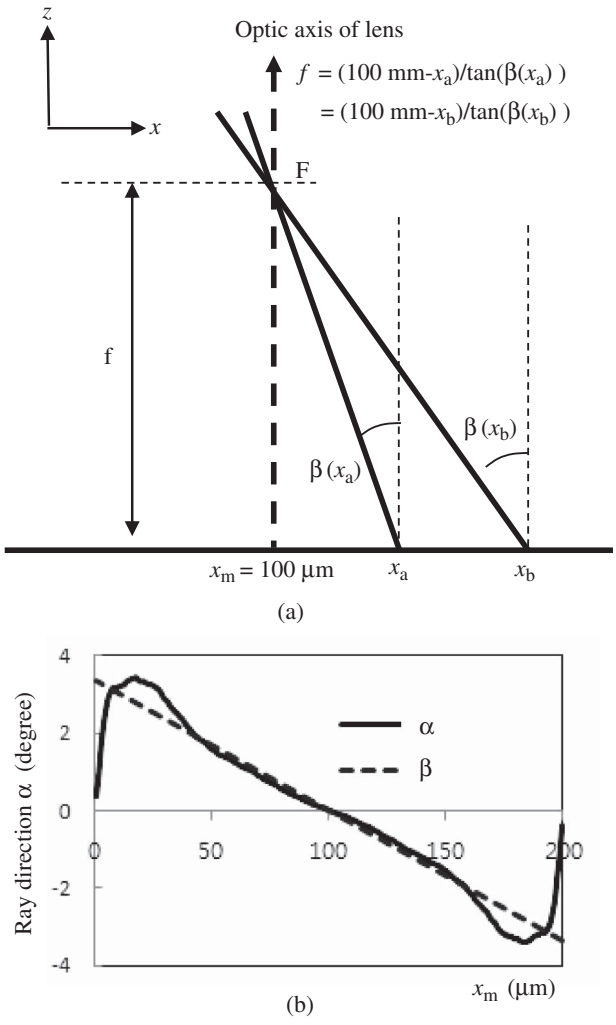

Figure 8. (a) Diagram showing that the right side of equation (6) should be equal to the focal length f if light rays of angle $\beta(x_m)$ intersect the optic axis at F irrespective of x_m. The x-coordinate of $x_m = 100$ μm is the center of the lens. (b) Comparison between angle α and β. The solid line represents angle α of the light rays from the ELC lens for the incident angle of 0°. The dotted line represents angle β which is equal to arctan((100 μm – x_m)/f).

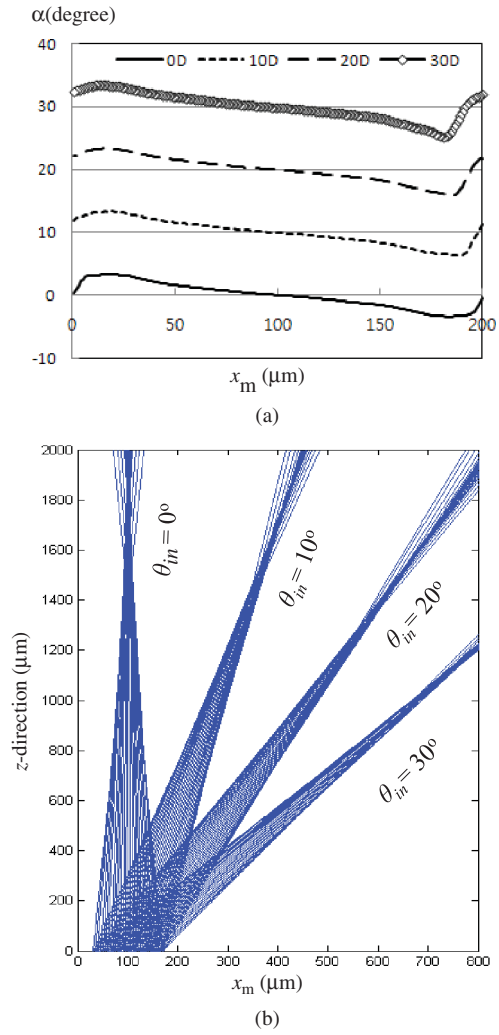

Figure 9. Comparison of the path of light rays for the various incident angles. (a) Angle of the light rays after the light passes through the ELC lens. Phase $kx_m\sin(\theta_{in})$ at the side of the lower substrate is included. Numbers on the upper side represent the incident angles. (b) Light rays after the light passes through the ELC lens on the zx-plane. The ELC lens is located at 0 mm in the z-direction and at x-coordinate ranges of 0–200 μm. Light passing through the x-coordinate ranges of 30–170 μm is represented in the figure.

are no longer linear and this implies that focusing characteristics will deteriorate. In Figure 9(b), light rays for the x_m range of 30–170 μm are illustrated. Figure 9(b) shows that the light rays gather at some position, but the z-coordinate of this position becomes smaller as the incident angle increases.

5. Conclusion

To investigate the performance of an ELC for various incident angles, a scheme to calculate the phase of the propagating light through an ELC lens was devised. The performance of ELC lens was characterised from the calculated directions of light rays.

The calculated results show that the performance of ELC lens in focussing light at one position decreases when the incident light is farther from the optic axis of the lens. The results for oblique incidence show that the focal distance decreases as the incident angle increases.

Acknowledgements

This study was financially supported by the Seoul National University of Science & Technology. The author also thanks the SANAYI system for the support of the Techwiz program.

References

[1] Javidi, B.; Okano, F. *Three-Dimensional Television, Video, and Display Technologies*; Springer: Berlin, 2002.

[2] The illustrated 3D HDTV list, in *The illustrated 3D movie list*, http://www.3dmovielist.com, accessed May 2012.

[3] Krijn, M.P.C.M.; de Zwart, S.T.; de Boer, D.K.G.; Willemsen, O.H.; Sluijter, M. *J. Soc. Inf. Disp.* **2008**, *16*, 847–855.

[4] Woodgate, G.J.; Harrold, J. *J. Soc. Inf. Disp.* **2006**, *14*, 421–426.

[5] Ren, H.; Fox, D.W.; Wu, B.; Wu, S.T. *Opt. Express* **2007**, *15*, 11328–11335.

[6] Kowel, S.T.; Cleverly, D.S.; Kornriech, P.G. *Appl. Opt.* **1984**, *23*, 278–289.

[7] Hong, H.K.; Jung, S.M.; Lee, B.J.; Shin, H.H. *J. Soc. Inf. Disp.* **2009**, *17*, 399–406.

[8] Sluijter, M.; Herzog, A.; de Boer, D.K.G.; Krijn, M.P.C.M.; Urbach, H.P. *J. Opt. Soc. Am. B* **2009**, *26*, 2035–2043.

[9] Ren, H.; Fan, Y.H.; Gauza, S.; Wu, S.T. *Jpn. J. Appl. Phys.* **2004**, *43*, 652–653.

[10] Lin, Y.H.; Ren, H.; Fan-Chiang, K.H.; Choi, W.K.; Gauza, S.; Zhu, X.Y.; Wu, S.T. *Jpn. J. Appl. Phys.* **2005**, *44*, 243–244.

[11] Yang, D.K.; Wu, S.T. *Fundamentals of Liquid Crystal Devices*; John Wiley & Sons: Chichester, 2006.

[12] http://www.sanayisystem.com, accessed May 2012.

[13] Gauza, S.; Zhu, X.; Wu, S.T.; Piecek, W.; Dabrowski, R. *J. Disp. Technol*. **2007**, *3*, 250–252.

[14] Hong, H.K. *Liq. Cryst.* **2011**, *38*, 689–696.

[15] Fowles, G.R. *Introduction to Modern Optics*; Holt Rinehart and Winston, Inc.: New York, 1975.